energies

Article

Optimal Sizing and Location of Photovoltaic Generation and Energy Storage Systems in an Unbalanced Distribution System

Ming-Yuan Chiang [1,*], Shyh-Chour Huang [1], Te-Ching Hsiao [1], Tung-Sheng Zhan [2,*] and Ju-Chen Hou [3]

1 Department of Mechanical Engineering, National Kaohsiung University of Science and Technology, Kaohsiung City 807618, Taiwan
2 Department of Electrical Engineering, National Kaohsiung University of Science and Technology, Kaohsiung City 807618, Taiwan
3 Department of Electrical Engineering, Kao-Yuan University, Kaohsiung City 82151, Taiwan
* Correspondence: j0933648904@gmail.com (M.-Y.C.); tszhan1109@nkust.edu.tw (T.-S.Z.)

Abstract: There has been an increasing number of renewable energy sources introduced into the distribution system to decrease the dependence on single power sources and relieve their effects related to global warming caused by power consumption. When greatly increasing renewable energy in the power system, the renewable energy connected to the power grid must be coupled with corresponding energy-storage technologies. This mechanism not only effectively improves the power floating problem but also more efficiently re-dispatches the power output. The purpose of this paper is to deal with the optimal sizing and location issue of the photovoltaic generation system and the battery energy storage system, which are proposed in order to improve the power loss, bus voltage profile, and voltage unbalance for the actual unbalanced loading distribution system of a large-scale chemical factory. The power loss, construction cost of the solar power and the energy storage systems, voltage variation ratio and voltage unbalance ratio will be treated as part of the objective function of the optimal problem. These variables are subject to various operating constraints and the voltage variation limit of the system when the photovoltaic generation and battery energy storage systems are operated. Furthermore, a refined genetic algorithm, which possesses an auto-selective crossover and mutation scheme, is proposed and applied in this paper in order to solve the optimization problem. Moreover, the simulation results are expected to demonstrate the superiority of the proposed algorithm.

Keywords: photovoltaic generation system; energy storage system; voltage unbalance ratio; voltage variation ratio; refined genetic algorithm

Citation: Chiang, M.-Y.; Huang, S.-C.; Hsiao, T.-C.; Zhan, T.-S.; Hou, J.-C. Optimal Sizing and Location of Photovoltaic Generation and Energy Storage Systems in an Unbalanced Distribution System. *Energies* **2022**, *15*, 6682. https://doi.org/10.3390/en15186682

Academic Editor: Surender Reddy Salkuti

Received: 11 August 2022
Accepted: 9 September 2022
Published: 13 September 2022

1. Introduction

In the recent decade, due to the government's policy promotion and people's recognition of energy-saving efforts and carbon emission reduction issues, more renewable energy sources have been introduced into the power distribution system to reduce the dependence on a single power source and alleviate global warming caused by electricity consumption. The majority of medium-and-above power users have decided to build renewable power generation sources in their factories, which provide the partial or whole daily system load demand [1–4], in line with the government's green energy policy. A renewable power source is directly integrated into the factory's power system to relieve the dependence on the power source that comes from the electrical utility, and to save electricity fees. Among the many renewable energy sources, solar power generation technology with relatively low installation costs has been developed rapidly. In particular, the photovoltaic generation system (PVGS) has become a widely considered renewable energy source for installation as a grid-connected and stand-alone power system [5,6].

In the current application of wind and solar power generation, besides the need to select an appropriate location and geographical conditions, the power generation time is limited by day and night power generation. It is also easily affected by the seasons and climate, which makes power generation unstable. If renewable power is integrated into the power system without any regulation, it will seriously affect the security and stability of the power. Therefore, the energy storage system (ESS) becomes a buffer or regulator before renewable energy is integrated into the power system, and is indispensable for a stand-alone microgrid. The battery energy storage system (BESS) is one of the most used energy storage systems that is easy and more convenient to operate than others. In particular, it can store unstable renewable energy power generation and turn it into a controllable power source [7–9]. While it serves as a stable power output, it also provides the function of eliminating the peak power demand of the system.

An optimization algorithm for sizing a PV-energy storage system for islands was proposed in [8]. The algorithm was developed to minimize the electricity generation cost by selecting the rated optimal power of the PV and the energy storage. Furthermore, a method of optimally selecting PV and battery sizes for residential grid-connected PV-battery systems was proposed in [9]. The paper used yearlong time series data while applying the genetic algorithm (GA) to minimize the total electricity cost for the whole year. The proposed algorithm selects the optimal number of PVs and batteries by varying the batteries' charging and discharging process based on solar availability and the time-of-use cost of electricity. The results of the proposed algorithm showed that co-optimizing the batteries and the PV sizes, which strongly depend on the residential load profile, could reduce the amount of electricity used by the houses from the grid as well as the overall annual cost of electricity. In reference [10], the main objective was to provide an electric supply to a residential complex located in a remote area in Iraq that has no access to the electricity grid. The nomadic people optimizer (NPO) was applied for the design of a stand-alone hybrid energy system (HES). The objectives of this study were to minimize the total life cycle cost, total dump energy, and total CO_2 emissions for 25 years. Reference [11] demonstrated that the unit sizing of a stand-alone wind–PV system simply requires an optimization task to determine the optimal generation capacity and battery storage for a typical load profile for a residential home constructed at a specific site located in remote hilly areas in Turkey's northwest Black Sea coast where no power grid is available. In the optimization process, the power demand, wind speed, and insolation rate are annually averaged hourly estimated values for the given system. Several combinations of PV alone, wind alone, and hybrid wind–PV systems are optimally sized to meet the load demand and minimize the total cost for a lifetime projection using the real-coded genetic algorithm (RCGA). However, the cases discussed in the above-mentioned references all employed residential or undeveloped areas as the research objects, and there is no relevant research and discussion on the power system of large-scale industrial users.

The heuristic algorithm can be classified into different categories according to these inspirations. These groups are evolutionary algorithms (EAs) such as genetic algorithms (GA) [12–16] and immune algorithms (IA) [17–19], or differential evolution mimicking the principles of the natural animal behavior evolutionary process to develop robust optimization techniques, such as particle swarm optimization (PSO) [20–22], the grasshopper optimization algorithm (GAO) [23], the firefly algorithm (FA) [24], the bee swarm optimization algorithm (BSOA) [25], and the bat algorithm (BA) [26]. In addition, many improved models have been proposed for the above optimization method [27–29], in order to improve the efficiency and accuracy of its solution. In this paper, the PVGS was the only renewable power source to supply power directly to the system load, after which the BESS would be installed in the same example system of a chemical factory. Therefore, it was necessary to investigate and analyze the effect of the feed-in location and installation capacity of the PVGS and BESS in the power system, in which the improvement of the system bus voltage profile and voltage unbalance for the system could be expected. The optimal decision mentioned above is an integer programming problem solved by a refined genetic algorithm with an auto-selective crossover and mutation scheme (RGA-ASCM). This programming problem was proposed in this paper to determine the optimal sizing and location issues for the newly constructed PVGS and BESS in an unbalanced three-phase distribution system of a large-scale chemical factory. The optimal decision problem is subject to all of the system constraints, including voltage variation limits, voltage unbalance limits, line capacity limits, and three-phase power balance equations [30,31], considering the goal of achieving system loss minimization and the lowest investment cost. The obtained results show that the optimal integration point of the PVGS is located close to the load, and the loss of the system line can be greatly reduced. However, due to its operational state, integrating the BESS will affect the behavior of the system voltage, power, voltage variation ratio (VVR), and system voltage unbalance ratio (VUR). According to the renewable energy power generation system connection grid code of the Taiwan Power Company (TPC), the VVR of the system's common coupling point is strictly limited to below 3.0%. Therefore, the proposed RGA-ASCM was compared with GA and IA under the same objective function and constraints in order to demonstrate its superior performance, and to converge to the optimal solution quickly and stably.

2. Problem Formulation

The sizing and location problems were modeled as an integer programming problem in order to determine the optimal feed-in location and installation capacity for both the PVGS and BESS. The above problem aims to minimize the power system loss and investment cost; VUR and VVR will be included in the objective function subject to all of the system operation equality and inequality constraints.

2.1. Objective Function

The optimal problem needs to minimize the investment cost of PVGS and BESS system installation, the system loss minimization, and the voltage operation indexes. The objective function can be formulated as

$$\text{Min. Obj}_F = F_{loss}(V,\ \theta) + F_{VUR}(V) + F_{VVR}(V) + FC_{pvgs}(Cap_{pvgs}) + FC_{bess}(Cap_{bess}), \quad (1)$$

$$F_{loss} = a \cdot \sum_t^T P_{lineloss}^t(V,\theta) + b \cdot \sum_t^T P_{Trloss}^t(V,\theta), \quad (2)$$

$$F_{VUR}(V) = \sum_t^T c^t \cdot \sum_{b=1}^{NB} VUR_b^t(V), \quad (3)$$

$$F_{VVR}(V) = \sum_t^T \sum_{b=1}^{NB} d_b^t \cdot VVR_b^t(V), \quad (4)$$

$$FC_{pvgs}(Cap_{pvgs}) = e \cdot \sum_{n=1}^{NS} Cap_{pvgs,n}, \quad (5)$$

$$FC_{bess}(Cap_{bess}) = f \cdot \sum_{m=1}^{NST} Cap_{bess,m}, \quad (6)$$

where

Obj_F	:	the objective function for the evaluation of the issue of sizing and locating.
F_{loss}	:	the function of system loss, including lines and transformers loss.
F_{VUR}	:	the summation function of the system voltage unbalance rate.
F_{VVR}	:	the summation function of the system voltage variation rate.
FC_{pvgs}	:	the installation cost of the PVGS.
FC_{bess}	:	the installation cost of the BESS.
VUR_b^t	:	the three-phase voltage unbalance rate on bus b at hour t.
VVR_b^t	:	the three-phase voltage variation rate on bus b at hour t.
a	:	the weighting parameter of the line power loss, 3×10^4(NT$/kW).
b	:	the weighting parameter of the transformer power loss, 3×10^4(NT$/kW).

c^t	:	the penalty parameter of the voltage unbalance rate at hour t (NT$). $c = \begin{cases} 9 \times 10^8 & \text{, if } VUR_b^t \geq VUR\_lim \\ 0 & \text{, if } VUR_b^t < VUR\_lim \end{cases}$ VUR_lim is the limitation of the voltage unbalance ratio on each load bus.
d_b^t	:	the penalty parameter of the voltage variation rate on bus b at hour t (NT$). $d = \begin{cases} 9 \times 10^8 & \text{, if } VVR_b^t \geq 3.0\% \\ 1 & \text{, if } VVR_b^t < 3.0\% \end{cases}$
e	:	the unit price of PVGS installation in NT$/kW.
f	:	the unit price of BESS installation in NT$/kWh.
$P_{lineloss}^t$	:	the total system line loss at hour *t* (kW).
P_{Trloss}^t	:	the total system transformer loss at hour *t* (kW).
$Cap_{pvgs,n}$	:	the PVGS capacity on the chosen bus n; it must be an integer in multiple numbers of 50 kW.
$Cap_{bess,m}$	:	the BESS capacity on the chosen bus m; it must be an integer in multiple numbers of 50 kW.
NS	:	the set of the chosen feed-in bus number of the PVGS.
NST	:	the set of the chosen feed-in bus number of the BESS.
NB	:	the maximum system bus number.

$P_{lineloss}^t$ and P_{Trloss}^t can be estimated by the three-phase power flow program. VUR_b^t is the voltage unbalance ratio, which can be calculated using the converged three-phase voltage of the power flow program [30,31] for each hour. According to the ANSI/IEEE standard, the voltage unbalance ratio is defined as

$$VUR = \frac{|V_{max} - V_{min}|}{V_{avg}} \times 100\%, \quad (7)$$

where

$$V_{avg} = \frac{(V_R + V_S + V_T)}{3}$$

V_R, V_S, and V_T are three-phase voltages, and V_{max} and V_{min} are the maximum and minimum phase voltage, respectively. VVR can be evaluated by Equation (8) with the voltage amplitude of the system's common coupling point with and without PVGS and/or BESS power injection, which are named V_{wt} and V_{wo}, respectively. When a power user installs a renewable energy power generation device, the VVR will be strictly limited by the power utility to a certain range, in order to avoid affecting the power quality.

$$VVR = \frac{|V_{wt} - V_{wo}|}{V_{wo}} \times 100\%, \quad (8)$$

2.2. Constraints

The following constraints must be satisfied:

(1) Equality constraints:

$$P_i = |V_i| \sum_{j=1}^{NB} |V_j||Y_{ij}| \cos(\theta_i - \theta_j - \theta_{ij}), \quad (9)$$

$$Q_i = |V_i| \sum_{j=1}^{NB} |V_j||Y_{ij}| \sin(\theta_i - \theta_j - \theta_{ij}), \quad (10)$$

P_i and Q_i are the bus's real power and reactive power, respectively. V and θ are the bus voltage and bus angle.

(2) Inequality constraints:

$$|S_{Tr.}^t| \leq S_{Tr.}^{Cap}, \quad (11)$$

$$\left|\overline{S}_{Line}^t\right| \leq S_{Line}^{Cap}, \quad (12)$$

$$0.95 \text{ pu} \leq |V_i| \leq 1.05 \text{ pu}, \quad (13)$$

$$\text{VVR} \leq 3.0\%, \tag{14}$$

where $\left|\overline{S}_{Tr.}^{t}\right|$ is the apparent power on the transformer at hour t, $S_{Tr.}^{Cap}$ is the rated apparent power capacity of the transformer, and $\left|\overline{S}_{Line}^{t}\right|$ and S_{Line}^{Cap} are the apparent line power and line capacity of the transmission line at hour t, respectively. Equations (11) and (12) indicate that the line power should be less than or equal to the rated line capacity. The bus voltage must operate between 0.95 pu and 1.05 pu, as shown in Equation (13). Furthermore, according to the renewable energy power generation system connection grid code of the TPC, the VVR of the system's common coupling point must be less than 3.0%, as described in Equation (14). All of the variables and indexes of the constraints mentioned above can be obtained or calculated from the rapidly converged three-phase power flow model developed by [30,31].

3. Solution Algorithm—RGA-ASCM

A genetic algorithm (GA) is a search algorithm based on the mechanism of natural selection and genetics [9–13]. A refined GA with an auto-selective crossover and mutation scheme (RGA-ASCM) was developed to enhance the performance of GA, as discussed in the following sections. Furthermore, the crossover and the mutation mechanism were refined by a competition and auto-selection scheme in order to avoid prematurity, and a competition mechanism was implemented to automatically determine the choice of either one or both. With the advantages of both heuristic ideals and AI, RGA-ASCM supersedes the original ideals threefold: the complicated problem can be solved, it can achieve better performance than GA, and it is more likely to reach a global optimum than heuristic methods.

3.1. Encoding of Genes and Chromosomes

The coding scheme of chromosomes is illustrated in Figure 1, where it was divided into two groups of chromosomes—one is for the determination of the sizing and location of PVGS, and the other is for BESS. The multiple integer numbers of the PVGS and BESS capacity were encoded into four-bit binary digits as the gene, then a chromosome was assembled by several genes' binary strings. Each chromosome indicates a combination of the integral multiple numbers of each specified bus. If the GA or RGA-ASCM search is terminated, each gene will then be decoded separately. For instance, in Figure 1, $\text{BIN\_PVGS}_i(\text{PN})$ is the binary string of PVGS on the i-th bus, and PN indicates the population index—, from 1 to the maximum population number.

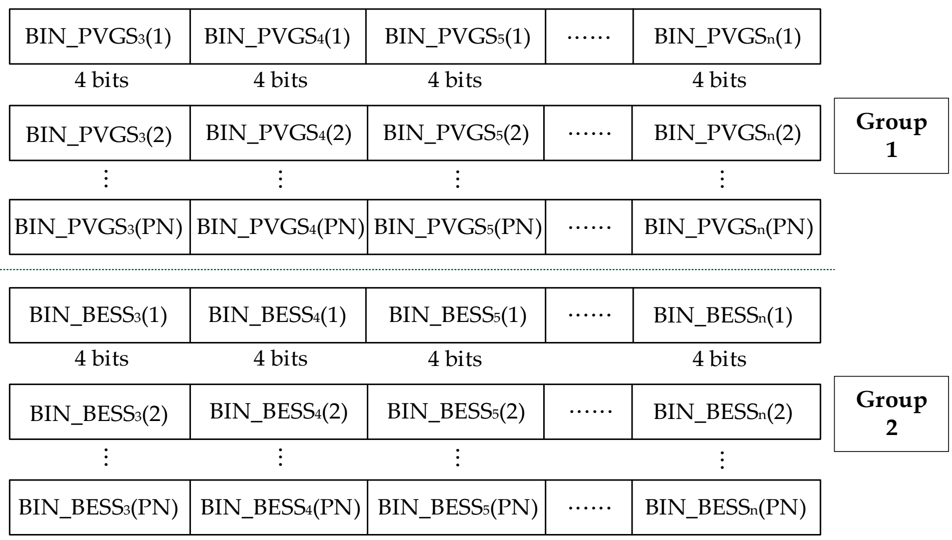

Figure 1. Genes on the chromosome strings.

3.2. Fitness Function Evaluation

The fitness score of each chromosome is obtained by calculating the objective function in Equation (1), considering the equivalent and inequivalent constraints mentioned in Equations (8)–(13). If one or more variables violate their limits, the corresponding genes will be placed into the tabu list in order to avoid infeasible solutions.

3.3. Production of the Offspring

The offspring are the new chromosomes generated from crossover and mutation processes. The crossover process is a structured recombination operation created by exchanging part of two chosen parent chromosomes. On the other hand, the mutation process is the occasional random inversion of the gene's binary digit of a single chromosome. These two operations are called simple crossover and mutation schemes (SCM), and the GA with SCM is shortened to SGA in this paper. In order to avoid the prematurity of the convergence of the SGA, an improved crossover and mutation (ICM) scheme is proposed instead of SCM, and is stated in detail in this section. These two schemes are described as follows:

1. SCM Scheme [12]

In the uniform probability distribution, the crossover process randomly selects two parents to exchange chromosomes with a crossover rate P_C. The location of the gene within the chromosome is called the loci. The crossover point is also randomly chosen from the loci. If one or both offspring is infeasible, another mate will be chosen again for crossover. On the other hand, the mutation process in the uniform probability distribution randomly selects one parent with a mutation rate P_M. The loci can be randomly selected for mutation. If the offspring is infeasible, another parent will be chosen until a feasible solution is obtained. In the SGA calculation process, the P_C and P_M are both fixed values between 0.0 and 1.0, and the P_C plus P_M must be equal to 1.0. The SGA has been described in detail in Ref. [12], so it will not be repeated in this paper.

2. ICM scheme

The crossover process generally executes before mutation throughout the SGA searching process. In the SGA, a higher crossover rate P_C allows the exploration of the solution space around the parent solution. The mutation rate P_M controls the probability of new genes being introduced, and explores new solution territory. If it is too low, the solution may settle at a local optimum. On the contrary, a high rate can generate too many possibilities of uncertainty. When the offspring lose their resemblance to their parents, the algorithm will not learn from the past, and can become unstable. Thus, it is a dilemma to choose a suitable crossover and mutation rate for the SGA. Hence, ICM was proposed to avoid such a difficulty, and is illustrated as follows:

(1) Select two parents randomly to produce offspring according to the following:
   (a) If $rand_C < {P_C}^{(g)}$ and $rand_M < {P_M}^{(g)}$, without executing the crossover and mutation processes;
   (b) If $rand_C \geq {P_C}^{(g)}$ and $rand_M < {P_M}^{(g)}$, only the crossover process is executed;
   (c) If $rand_C < {P_C}^{(g)}$ and $rand_M \geq {P_M}^{(g)}$, only the mutation process is executed;
   (d) If $rand_C \geq {P_C}^{(g)}$ and $rand_M \geq {P_M}^{(g)}$, with the crossover and mutation process executed sequentially.

where

$rand_C$	:	the uniform random number in (0,1) for crossover.
$rand_M$	:	the uniform random number in (0,1) for mutation.
g	:	the current generation numbers.
${P_C}^{(g)}$	:	the control parameter crossover process with initial value ${P_C}^{(0)} = 0.5$ and $0 \leq P_C \leq 1$.
${P_M}^{(g)}$	:	the control parameter mutation process with initial value ${P_M}^{(0)} = 0.5$ and $0 \leq P_M \leq 1$.

The offspring will be generated until all of the parents are processed. Figure 2 shows the initial relationship bet crossover and mutation in ICM with three procedures: crossover, mutation, and both, which can be performed to generate offspring in equal initial probability. If the random number of crossovers or mutations is less than the corresponding control parameter, the related procedures will not be implemented. The mutation operation plays a more important role than that in SGA, as the mutation is more capable of exploring new regions. If the search is very close to the local or global optimum, the mutation may need to become dominant, especially in the absence of critical good genes in a generation. As all of the procedures are random operators, there is no telling which one is better than the other two.

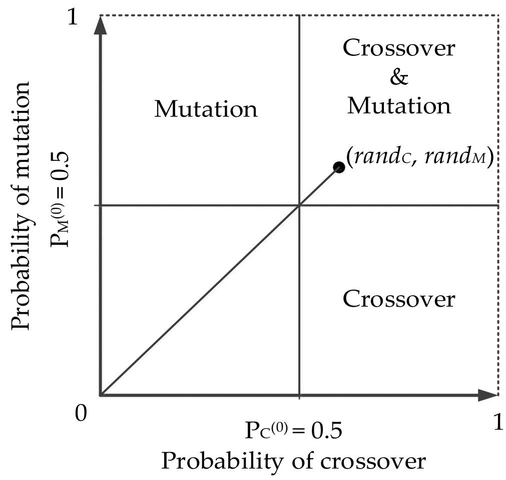

Figure 2. Initial probability map of the crossover and mutation in ICM.

(2) A competition mechanism is implemented in the searching process according to the fitness score. For instance, if the best current solution comes from both the crossover and mutation processes, there is more likelihood for this procedure to generate better offspring for the next population. The area of the crossover and mutation procedure must be increased by reducing $P_C{}^{(g)}$ and $P_M{}^{(g)}$ to expand the probability, as shown in Figure 3.

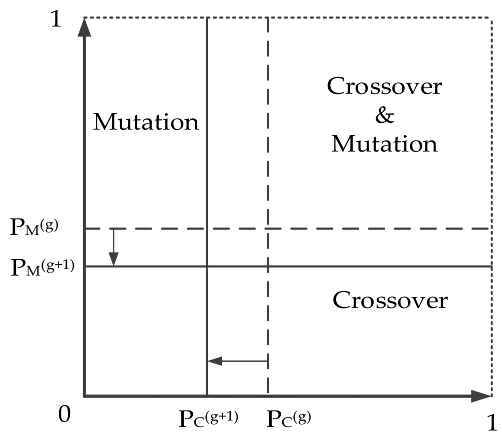

Figure 3. Variation for increasing crossover and mutation probability.

If the best fitness of generation g-1 is greater than that of generation g (i.e., $\text{Obj}_{\text{Fmin}}^{(g-1)} > \text{Obj}_{\text{Fmin}}^{(g)}$ comes from the crossover and mutation procedure), both control parameters will decrease, which is demonstrated as follows:

$$P_C^{(g+1)} = P_C^{(g)} - D_1 = P_C^{(g)} - \left(\frac{K_1}{g_{\max}}\right), \tag{15}$$

$$P_M^{(g+1)} = P_M^{(g)} - D_2 = P_M^{(g)} - \left(\frac{K_2}{g_{max}}\right), \quad (16)$$

where K_1 and K_2 are the regulating factors, and in general, $K_1 < K_2$. g_{max} is the maximum generation number. Figure 3 shows the variation in the probability of the crossover and mutation areas. On the contrary, there is a greater likelihood for the other two procedures to generate better offspring, in which both control parameters must increase in order to diminish the probability, as shown in Figure 4. If the best solution remains the same, the operation of the crossover and mutation also needs to hold back in order to recover the related area. If the best fitness of generation g-1 is less than that of generation g (i.e., $Obj_{Fmin}^{(g-1)} \leq Obj_{Fmin}^{(g)}$ comes from the crossover and mutation), the control parameters will increase in the following manner:

$$P_C^{(g+1)} = P_C^{(g)} + D_1, \quad (17)$$

$$P_M^{(g+1)} = P_M^{(g)} + D_2, \quad (18)$$

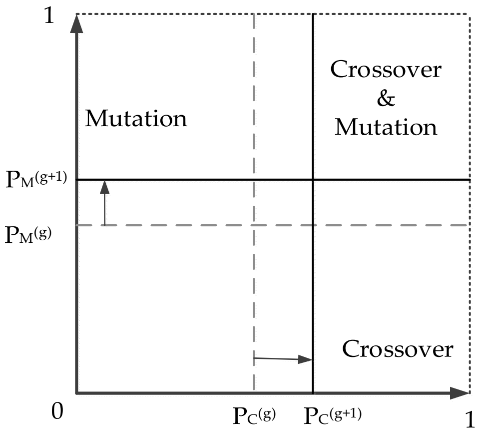

Figure 4. Variation for decreasing crossover and mutation probability.

It is worth noting that there is no restriction that P_M plus P_C must be equal to 1.0 in the ICM process, and it is not difficult to find that these two variables will operate independently from Equations (15)–(18).

(3) If the best fitness of generation g-1 is greater than that of generation g (i.e., $Obj_{Fmin}^{(g-1)} > Obj_{Fmin}^{(g)}$ comes from only the crossover procedure), the control parameter will decrease by using Equation (15). Conversely, if $Obj_{Fmin}^{(g-1)} \leq Obj_{Fmin}^{(g)}$ comes from the crossover, the control parameters will increase by employing Equation (17). In this situation, the control parameter P_M is fixed. The probability variation of the crossover is illustrated in Figures 5 and 6.

(4) If the best fitness of generation g-1 is greater than that of generation g (i.e., $Obj_{Fmin}^{(g-1)} > Obj_{Fmin}^{(g)}$ comes only from the mutation procedure), the control parameter will decrease by employing Equation (16). Conversely, if $Obj_{Fmin}^{(g-1)} \leq Obj_{Fmin}^{(g)}$, the control parameters will increase by employing Equation (18). In this situation, the control parameter P_C is fixed. The probability variation is illustrated in Figures 7 and 8.

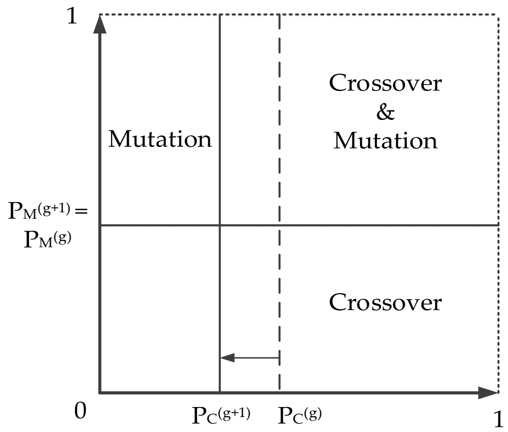

Figure 5. Variation for increasing crossover probability.

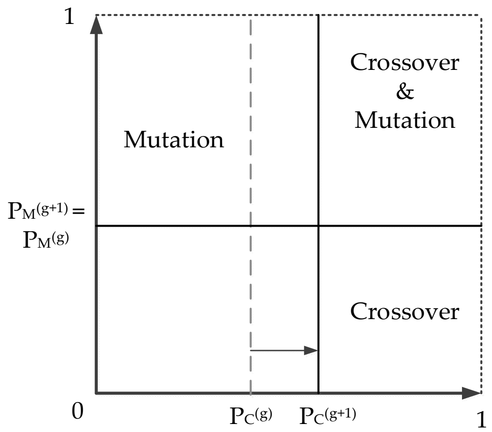

Figure 6. Variation for decreasing crossover probability.

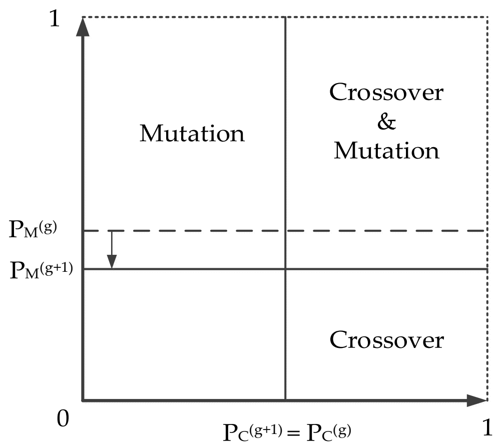

Figure 7. Variation for increasing mutation probability.

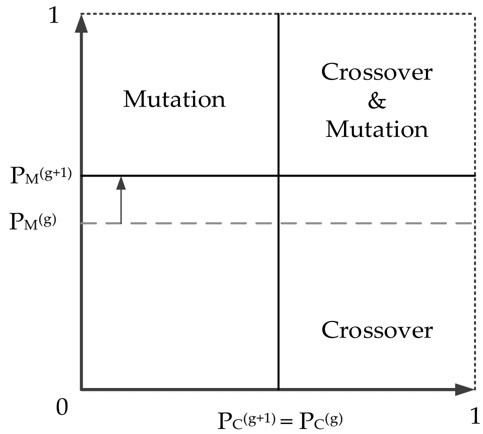

Figure 8. Variation for decreasing mutation probability.

3.4. Tabu List

A tabu list is introduced in order to avoid forbidden moves, such as

- The solutions just visited, except for the best solution in the current generation;
- Any local optima ever visited;
- The chromosomes violate the constraints;
- The solution space cannot accord with the bargain condition.

3.5. Elitism Selection

The 2k chromosomes, including p parents and p offspring, are then ranked in descending order according to their fitness values. "h" individuals with the best fitness are kept as the parents for the next generation. Other individuals in the combined population of size (2k-h) have to compete by adopting the roulette wheel approach to be selected for the next generation.

3.6. Stopping Rule

The process of generating new trials with the best fitness is continued until the fitness values are optimized or the maximum generation number is reached. The steps of the RGA-ASCM process are shown below:

- Step 1. Data Collection.
- Step 2. Randomly generate the multiple integer numbers of the PVGS and BESS capacity;
- Step 3. Coding—decimal to four-bit binary digits;
- Step 4. ICM process;
- Step 5. Decoding—four-bit binary digits to decimal;
- Step 6. Check if the chromosomes are in the Tabu list;
- Yes: Go to Step 4; No: Go to Step 7;
- Step 7. Elite selection;
- Step 8. Did the convergence occur? Or is the maximum generation number reached?
- Yes: Go to Step 9; No: Go to Step 4;
- Step 9. List the optimal planning combinations;
- Step 10. End.

4. Simulation and Discussion

The proposed algorithm was applied for the determination of the optimal sizing and location issue of a 32-bus test system in a chemical factory, with the intent to reduce the total active power loss, improve voltage unbalance, and minimize investment costs. The 32-system structure is shown in Figure 9; only one single power source, the Taiwan Power Company (TPC), exists in this system, with one main substation, fifteen load buses, and fifteen distribution transformers. The main substation consists of a 69 kV/11.4 kV, 30 MVA, Delta-Wye connection transformer. The optimal sizing and location problem solved by

RGA-ASCM was coded by MATLAB software, and all of the programs were executed on a personal computer with Intel Core i5-6500 3.2 GHz CPU and 16.0 GB RAM. The total system active and reactive load curves at Bus 1 for the original case of uninstalling PVGS and BESS units are shown in Figures 10 and 11, respectively. It is noteworthy that the system has a three-phase unbalanced load.

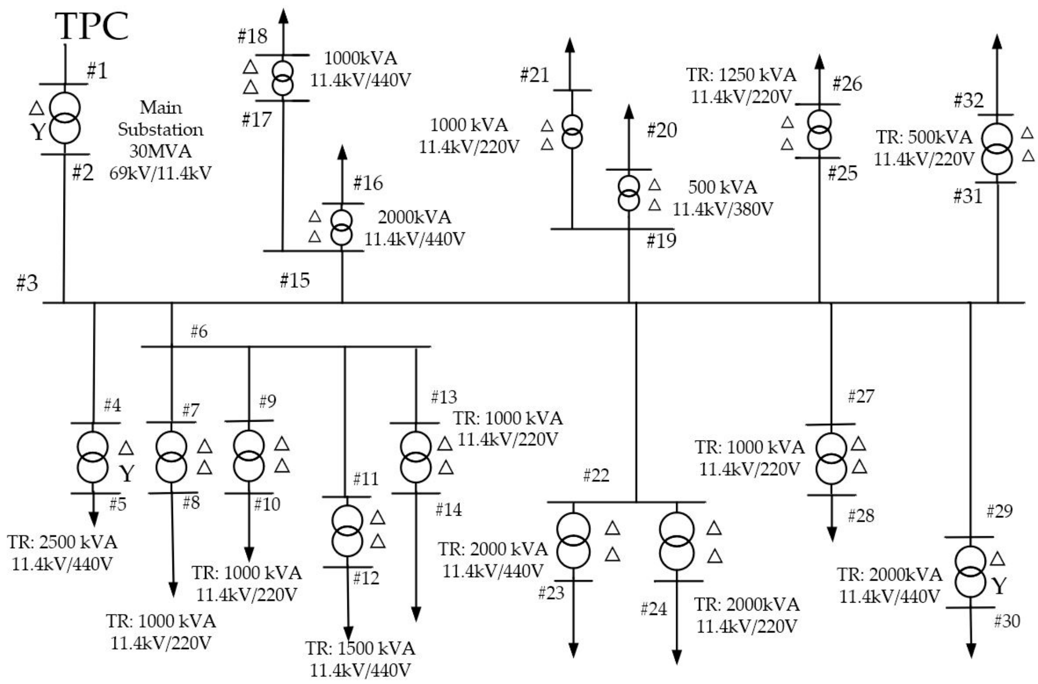

Figure 9. The 32-bus system of a chemical factory.

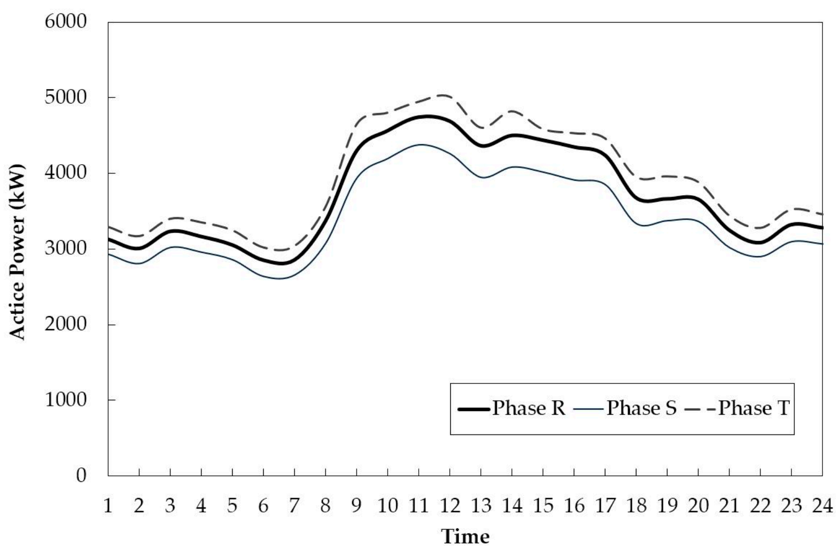

Figure 10. Daily unbalanced three-phase active power consumption at Bus 1.

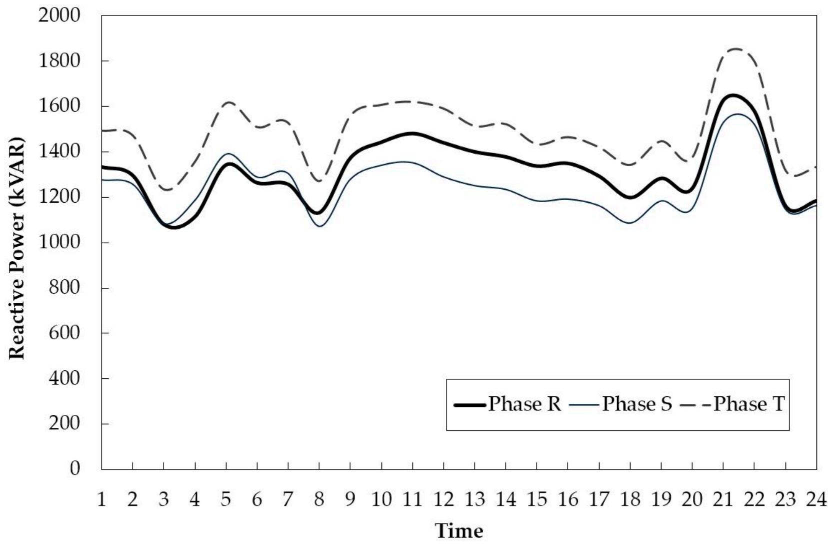

Figure 11. Daily unbalanced three-phase reactive power consumption at Bus 1.

4.1. Generation Curve of PVGS

By considering the PVGS injection, the PV generation model [32] can be found, as shown in Figure 12. This curve was actually measured in the Luzhu District of Kaohsiung city of the Republic of China, and the measurement time was July 2018. Southern Taiwan has more than 280 sunny days in a year. This figure is a base case and a normalized generation curve of a 50-kW solar power system. It can be seen that solar power systems can maintain more than 60% of the rated output power between AM 8:00 and PM 5:00. The integral multiple numbers of 50kW are mentioned in Equation (5), and BIN_PVGS_i in Section 3.1 is investigated by the RGA-ASCM.

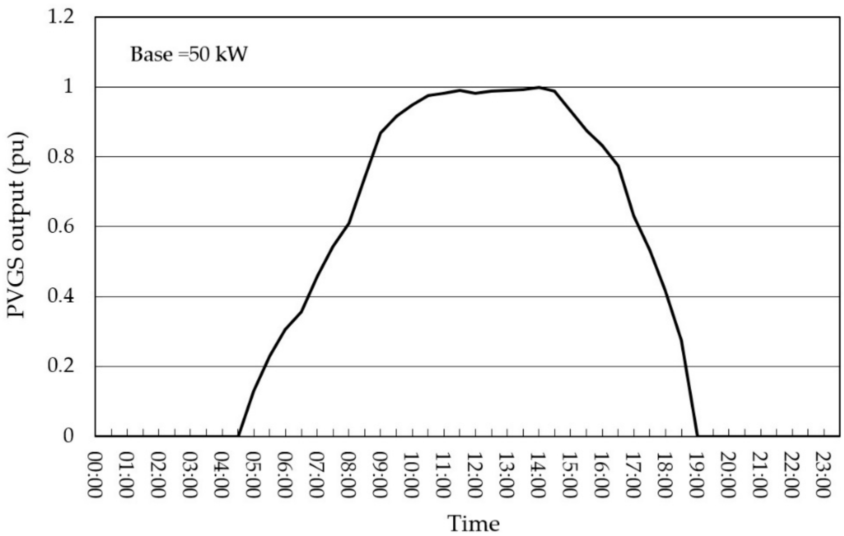

Figure 12. The normalized power curve of a 50-kW solar panel.

4.2. Operation Curve of the BESS

The BESS can store unstable renewable energy and turn it into a controllable power source. Not only does it serve as a stable power output, it also provides the function of eliminating the peak load demand of the system. Figure 13 shows a pre-specified normalized operation curve of a 50 kW BESS. The integral multiple numbers of 50 kW are mentioned in Equation (6), and BIN_BESS_i in Section 3.1 is also determined by the RGA-

ASCM. The curve can be customized through the BESS controller. A different operation curve will affect the results of the BESS sizing planning.

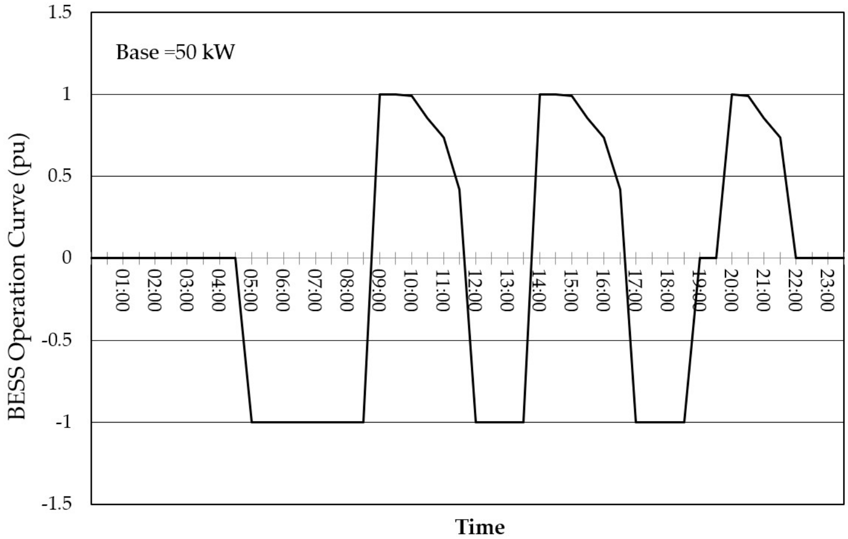

Figure 13. The normalized operation curve of a 50-kW BESS.

4.3. Optimal Sizing and Locating Combinations of the PVGS and BESS

In highlighting the impact of integrating the PVGS and BESS on the distribution system, three conditions were tested in this paper: Case 1—the original situation without any extra integration; Case 2—minimization in Equation (1) was considered with constraints, as in Equations (7)–(13) except for the BESS construction cost; and Case 3—based on Case 2, with the BESS construction cost included. The optimal solution of the RGA-ASCM in the last two cases is shown in Tables 1 and 2.

Table 1. The optimal solution for PVGS sizing and the location of Case 2 and Case 3.

Bus		**3**	**4**	**5**	**6**	**7**	**8**	**9**	**10**
PVGSCapacity(kW)	**Case 2**	0	250	0	600	0	0	0	0
	Case 3	400	250	0	250	0	0	0	0
Bus		**11**	**12**	**13**	**14**	**15**	**16**	**17**	**18**
PVGSCapacity(kW)	**Case 2**	0	0	0	0	600	0	250	0
	Case 3	0	0	250	0	400	500	250	0
Bus		**19**	**20**	**21**	**22**	**23**	**24**	**25**	**26**
PVGSCapacity(kW)	**Case 2**	750	0	0	500	0	0	400	0
	Case 3	250	250	0	100	350	0	300	0
Bus		**27**	**28**	**29**	**30**	**31**	**32**	**Total Cap.**	
PVGSCapacity(kW)	**Case 2**	350	0	400	0	400	0	4500	
	Case 3	250	0	250	0	250	0	4300	

The results indicate that although Case 3 was based on all of the conditions of Case 2, it was not difficult to determine that the PVGS installation capacity of Case 2 on almost all of the buses was bigger than the capacity of Case 3 in Figure 1. In addition, the BESS installation capacity, as shown in Table 2, was introduced to share the load demands according to the operation curve, as illustrated in Figure 9. The total installed capacity of the BESS was almost about 88% of the PVGS capacity for improving VUR and power loss. While the larger capacity of the PVGS and BESS installation may promote power quality, higher installation and construction costs were required.

Table 2. The optimal solution for the BESS sizing and the location of Case 3.

Bus		3	4	5	6	7	8	9	10
BESS Capacity (kW)	**Case 3**	350	200	0	200	0	0	0	0
Bus		**11**	**12**	**13**	**14**	**15**	**16**	**17**	**18**
BESS Capacity (kW)	**Case 3**	150	0	100	0	300	300	200	0
Bus		**19**	**20**	**21**	**22**	**23**	**24**	**25**	**26**
BESS Capacity (kW)	**Case 3**	200	200	0	100	300	0	250	0
Bus		**27**	**28**	**29**	**30**	**31**	**32**	**Total Cap.**	
BESS Capacity (kW)	**Case 3**	250	0	250	200	250	0	3800	

4.4. Analysis of the Voltage Variation Rate

The 24-h three-phase voltage profile comparisons between each test condition are shown in Figures 14–17 for Bus 1 and Bus 22. Bus 1 is the system's common coupling point of the chemical factory, and Bus 22 is chosen for demonstration due to the heavy loading bus. Notably, the VVR of Bus 1 must be less than 3% in order to comply with the TPC grid code requirement. Figures 14 and 15 illustrate the comparison of the three-phase voltages on Bus 1 and Bus 22 under the conditions of Case 1 and Case 2, respectively. Case 2 only considered the integration of the PVGS, such that the system voltage is a clear upward trend between AM4:30 and PM7:00. Furthermore, Figures 16 and 17 also show the comparison of the voltage variation on the same buses for the conditions of Case 1 and Case 3, respectively. In Case 3, the integration of the PVGS and the BESS was considered, such that the charging and discharging operation of the BESS resulted in voltage promotions.

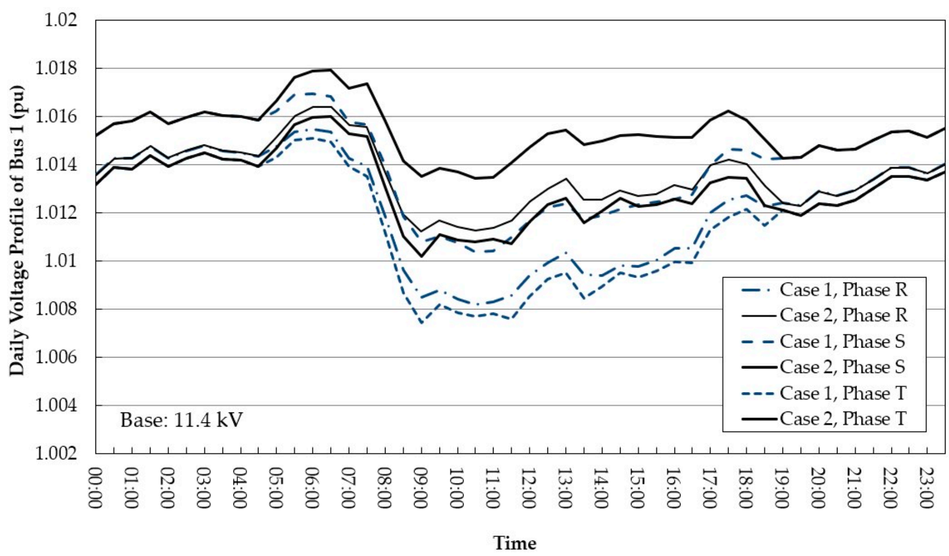

Figure 14. Voltage variation comparison on Bus 1 for Case 1 and Case 2.

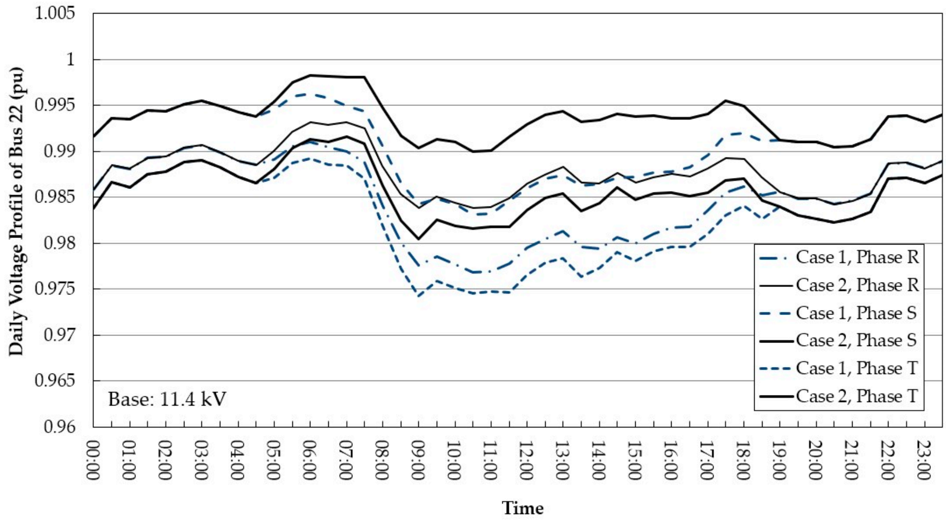

Figure 15. Voltage variation comparison on Bus 22 for Case 1 and Case 2.

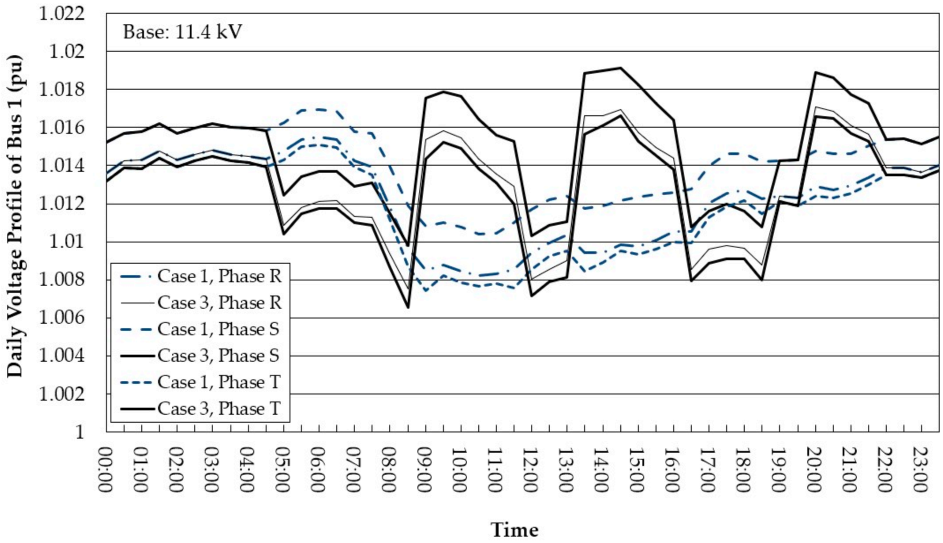

Figure 16. Voltage variation comparison on Bus 1 for Case 1 and Case 3.

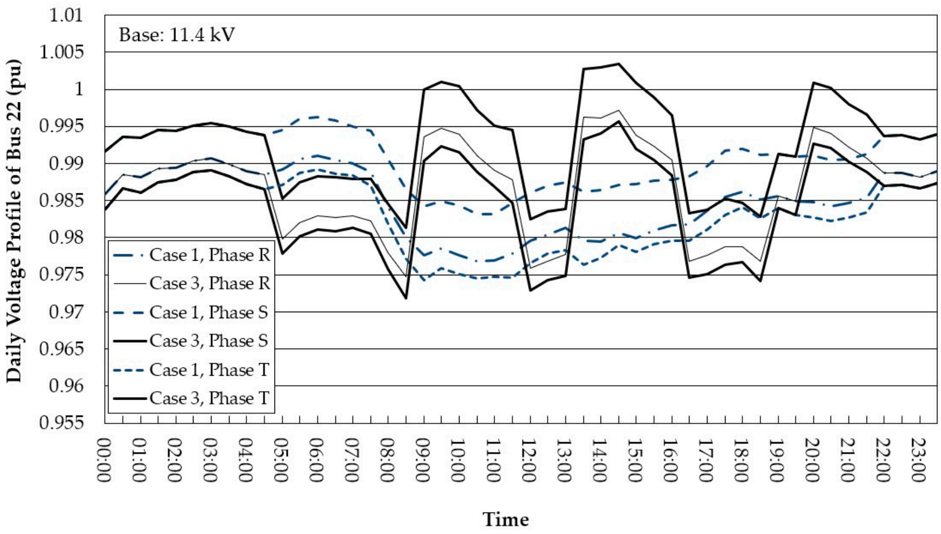

Figure 17. Voltage variation on Bus 22 for Case 1 and Case 3.

The 24-h VVR curves of Bus 1 and Bus 22 for Case 2 are demonstrated in Figures 18 and 19, respectively. Because only the PVGS injection was considered, the VVR only occurred during the day when there was sufficient sunlight. Figures 20 and 21 show the daily VVR curves for Case 3, illustrating that the VVR had a higher variation than that of Case 2 due to the PVGS and BESS being injected with power at the same time. All of the trends of the VVR curves have a certain correlation with the PVGS curve and BESS operation curve, as demonstrated in Figures 12 and 13.

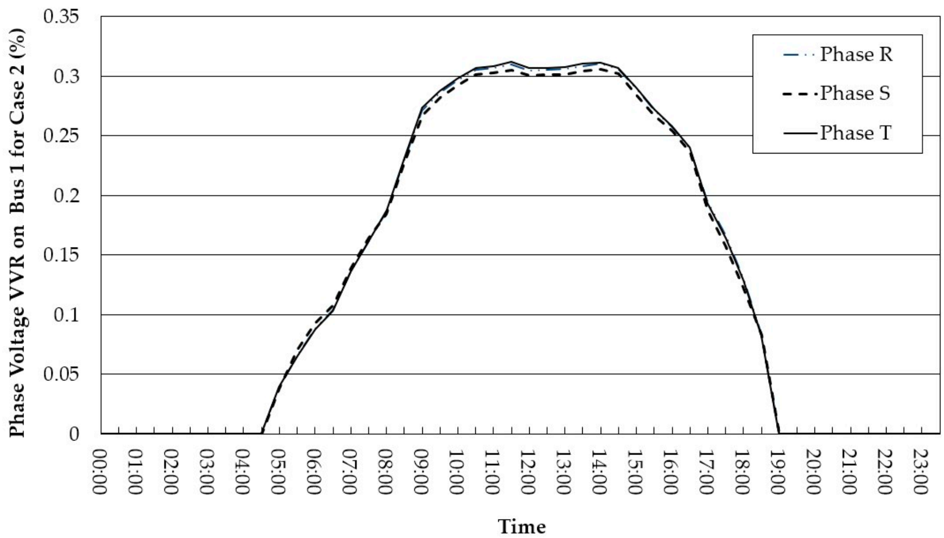

Figure 18. Three-phase VVR variation on Bus 1 for Case 2.

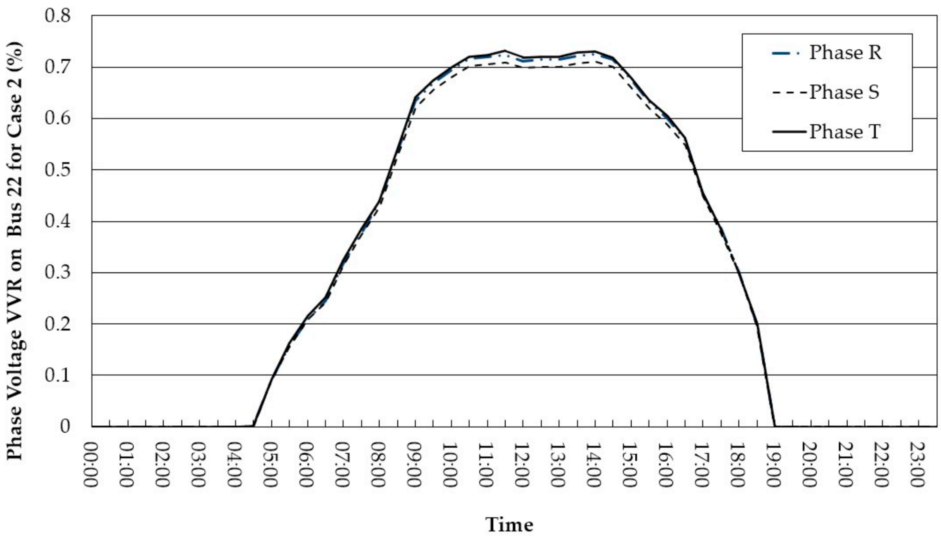

Figure 19. Three-phase VVR variation on Bus 22 for Case 2.

No matter which scenario it is, the VVR on Bus 1 can comply with the grid code of the TPC. When the system is in the planning stage, it will simulate a more extreme situation in order to test whether the system can still comply with the specifications of the system security grid code when the PVGS and BESS inject power at the same time. However, during actual operation, the BESS can adjust the power supply capacity and power supply duration through the system controller in order to avoid substantial changes in the system voltage.

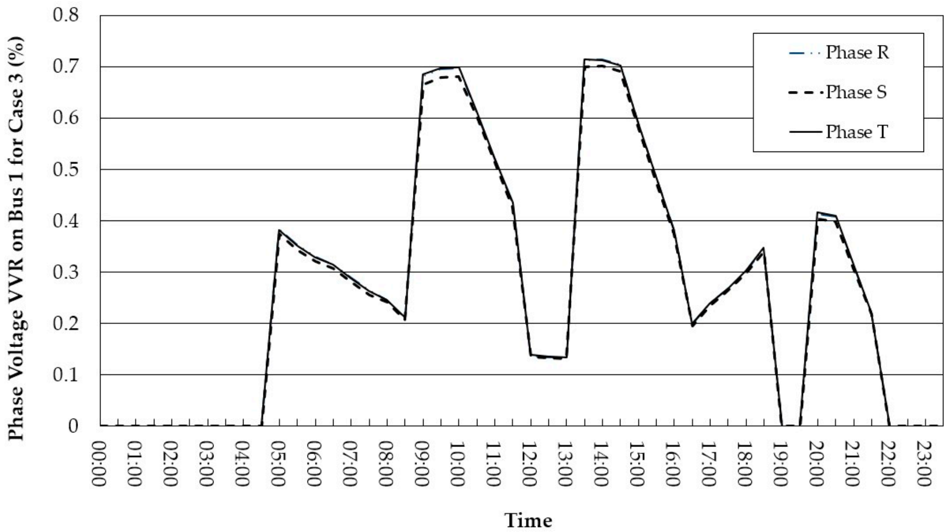

Figure 20. Three-phase VVR variation on Bus 1 for Case 3.

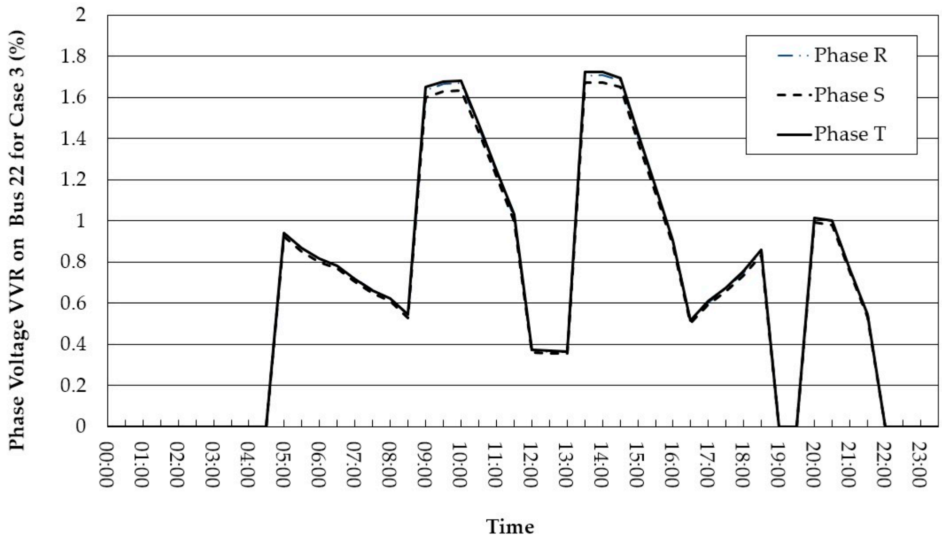

Figure 21. Three-phase VVR variation on Bus 22 for Case 3.

4.5. Analysis of the Voltage Unbalance Rate

Figures 22 and 23 show the variation of the VUR on Bus 1 and the heavily loaded Bus 22 in the three scenarios. It was found that the VUR of Case 2 was improved compared to Case 1. However, the curves presented by Case 3 might not be completely consistent when the BESS was charging during certain periods. In these periods with higher VUR, the BESS can be regarded as a load of the system that increases the VUR until it switches to the discharge mode, effectively reducing the VUR.

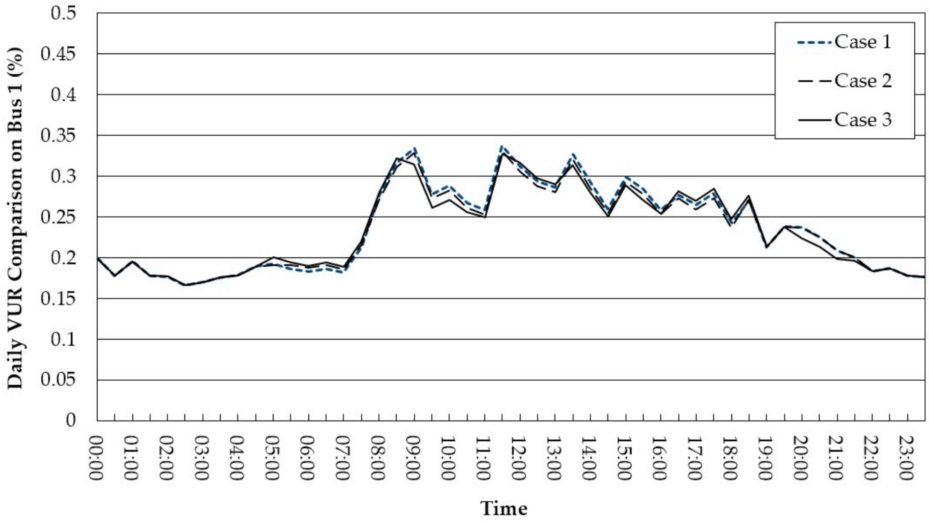

Figure 22. Daily VUR curve comparison on Bus 1.

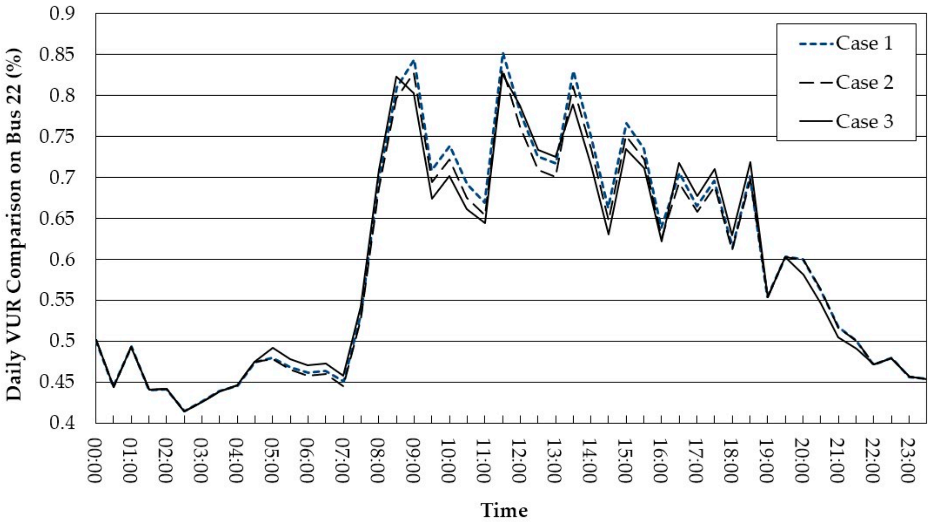

Figure 23. Daily VUR curve comparison on Bus 22.

4.6. System Cost and System Loss

In this paper, it was assumed that the unit capacity price of PVGS and BESS are NT $3,500,000 per 50 kW and NT $2,700,000 per 50 kW [32], respectively. The total installation costs in Case 2 and Case 3—as solved by SGA, IA and RGA-ASCM—are shown in Table 3. As for the results of Case 2 or Case 3, the RGA-ASCM proposed in this paper can find a better solution, resulting in a lower investment cost.

Table 3. Comparison of the total installation cost in Case 2 and Case 3.

Case	Algorithm	Total PVGS Installation Capacity (kW)	Total BESS Installation Capacity (kW)	Total Installation Investment Cost (NT$)
2	SGA	4950	–	345,600,000
	IA	5300	–	371,000,000
	RGA-ASCM	4500	–	315,000,000
3	SGA	4650	3950	538,800,000
	IA	4800	4050	554,700,000
	RGA-ASCM	4300	3800	506,200,000

According to the simulation result, the PVGS could reduce the power consumption from the power utility during the daytime. However, Case 3 considers the power generation injection of the PVGS and BESS at the same time, the trend of their real power consumed also varied with the charging/discharging operation curve of the BESS mentioned in Figure 9. The real power requirement of the entire system increases when the BESS is charging, but the requirement decreases when the BESS is discharging (supplying power). The comparison of the total power consumption of the system in each scenario is shown in Figure 24. In the figure, Case 2 alone considered the PVGS integration, which could have a larger decrease compared to Case 1. On the other hand, in Case 3, because the BESS needs to be charged, there will be a certain degree of power consumption leading to the reduction of the power saving. However, the energy consumption is just a little higher than that in Case 2. This situation can also be verified by the three-phase active power loss under various test scenarios in Figure 25.

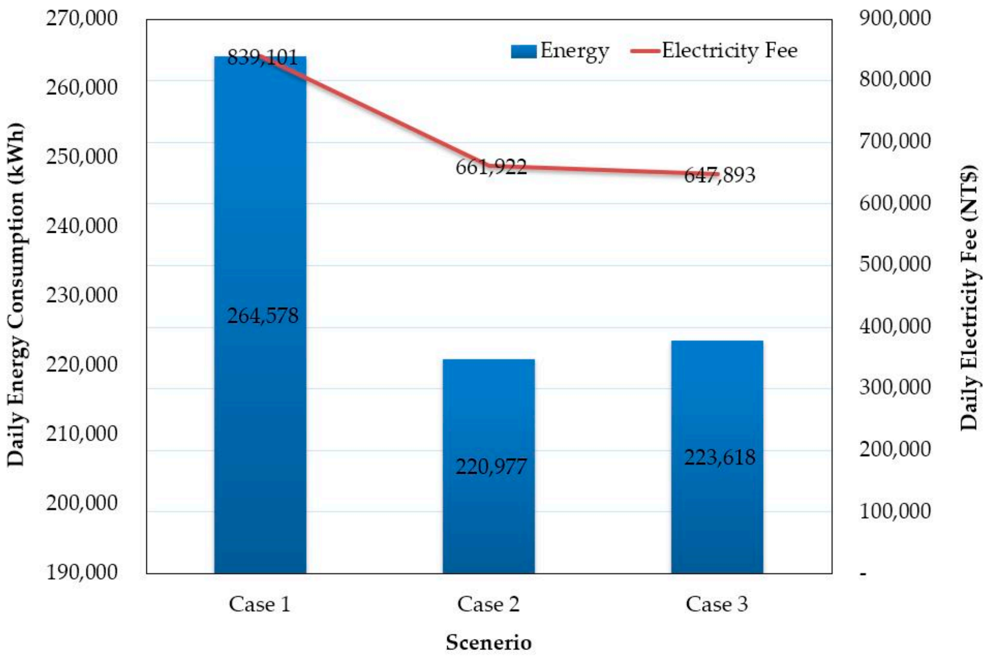

Figure 24. Comparison of the energy consumption and electricity fee for each scenario.

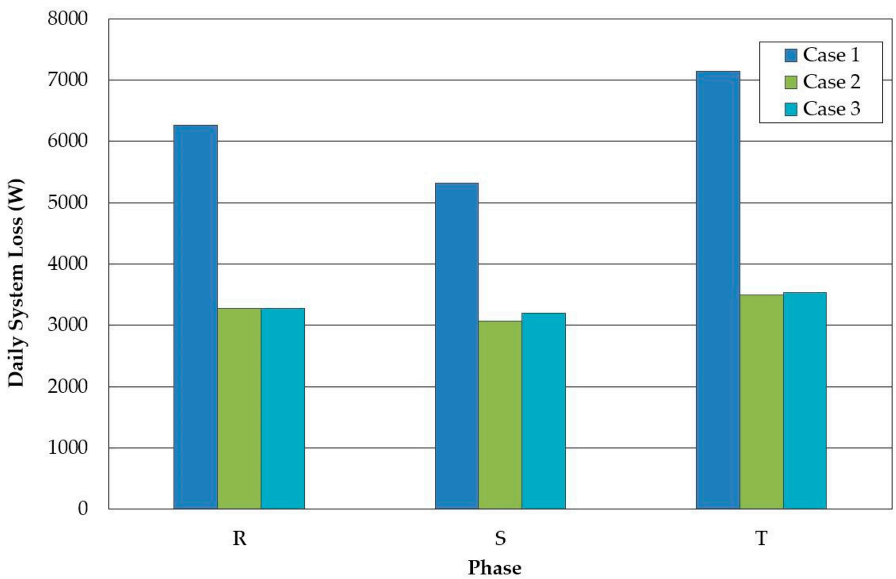

Figure 25. Comparison of the system total power loss for each scenario.

The chemical factory adopted the three-stage electricity pricing model as the electricity calculation method. The pricing model was divided into peak, half-peak and off-peak sections, and the prices of the three sections are shown in Table 4. The daily electricity fee for the three scenarios is also shown in Figure 24; the BESS charged by the PVGS in daytime, then it injects power to eliminate the peak load of the system for the duration of the higher electricity price to reduce electricity bills.

Table 4. The price of the three-stage electricity pricing model.

Section Name	Time Section	Price
peak	AM 10:00–PM 12:00$$PM 01:00–PM 05:00	NT $4.61/kWh
half-peak	AM 07:30–AM 10:00$$PM 12:00–PM 01:00	NT $2.87/kWh
off-peak	AM 00:00–AM 07:30$$PM 10:30–AM 00:00	NT $1.29/kWh

4.7. Convergence Performance of the RGA-ASCM

The performance of the RGA-ASCM, GA, and IA in searching for the best solution for optimal locating and sizing is presented in Figure 26. These heuristic search methods were tested based on the same fitness function and constraint set, and then the convergence diagrams were drawn from the average value of each method after executing the corresponding program 30 times, with each time having 200 chromosome populations for 100 iterations. Figure 26 demonstrates that the proposed RGA-ASCM can obtain the best solution in the 37th generation (or iteration), and that it performs better than the other two algorithms in finding the minimum fitness value. Moreover, it obtains the best combination of the PVGS and BESS installation, and the approximate lowest investment cost for each scenario.

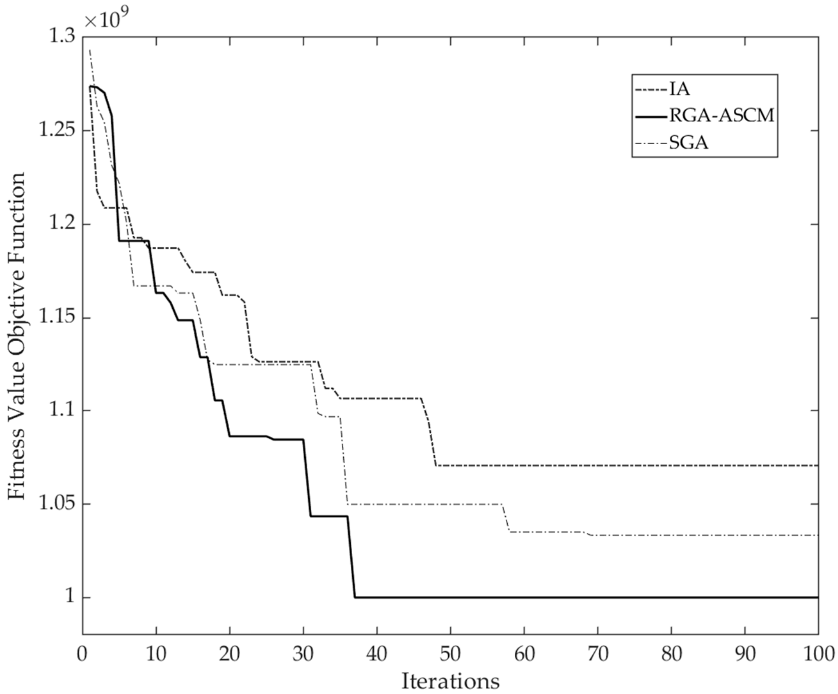

Figure 26. Convergence diagram comparison in 100 generations (iterations) for Case 3.

5. Conclusions

In this paper, an actual unbalanced three-phase power distribution system of a large-scale factory was taken as an example in order to demonstrate how the locating and sizing of PVGS and BESS can be performed on this system. A refined GA algorithm, named RGA-ASCM, was proposed in order to deal with the optimal locating problem and the integer programming problem of device capacity sizing optimization. When the power system was under a heavy load during the day, the electrical utility scattered PVGS and BESS supplied power simultaneously, diminishing the electricity payments, lessening system losses, and improving the three-phase voltage unbalance rate. The voltage variation data simulated in this paper show that PVGS can increase the system voltage between 6:00 am and 7:00 pm under sufficient sunshine conditions. In addition, according to the simulation results of the 24-h variation of VUR in each scenario, the power supply time of PVGS can suppress the voltage unbalance rate in the system, reduce the demand for electrical utility, and save electricity expenses. Furthermore, because the optimal integration point of the PVGS is located close to the load, the loss of the system line can be greatly reduced. On the other hand, integrating BESS will affect the behavior of the system voltage, power, VVR, and VUR due to its operational state.

Moreover, the proposed RGA-ASCM can automatically adjust the probability of the crossover and mutation in the algorithm during the solution process. As the simulation result of this paper, we chose to compare GA and IA under the same objective function and constraints. We found that the RGA-ASCM has better performance and can converge to the optimal solution quickly and stably. In terms of construction costs, the additional construction of the PVGS and BESS requires a considerable investment cost, which merits comprehensive planning in the early stage of construction. Building a PVGS and BESS needs to be a trade-off, considering the balance between the payback period of electricity payments, the power system quality, and the equipment investment cost.

Author Contributions: Conceptualization, M.-Y.C. and T.-S.Z.; methodology, T.-S.Z.; software, T.-S.Z. and J.-C.H.; validation, S.-C.H.; formal analysis, M.-Y.C.; investigation, M.-Y.C.; resources, M.-Y.C.; data curation, J.-C.H.; writing—original draft preparation, T.-C.H.; writing—review and editing, T.-S.Z. and T.-C.H.; supervision, S.-C.H.; funding acquisition, M.-Y.C. and T.-S.Z. All authors have read and agreed to the published version of the manuscript.

Funding: The work of T.-S.Z. was funded by the Ministry of Science and Technology of Taiwan, R.O.C. under Grant MOST 108-2221-E-244-003.

Institutional Review Board Statement: Not applicable.

Informed Consent Statement: Not applicable.

Data Availability Statement: Not applicable.

Acknowledgments: The author would like to thank the financial support given to this work by the Ministry of Science and Technology, Taiwan, R.O.C. under contract number MOST 108-2221-E-244 -003 is appreciated.

Conflicts of Interest: The authors declare no conflict of interest.

References

1. Tsai, M.T.; Chen, S.L.; Wu, S.W.; Lin, C.P. The optimal placement of wing turbine in a distribution system. In Proceedings of the 2nd International Conference on Intelligent Technologies and Engineering Systems (ICITES 2013), Kaohsiung City, Taiwan, 2–14 December 2013.
2. Zhang, Y.; Yao, F.; Iu, H.H.; Fernando, T.; Trinh, H. Operating optimization of wind-thermal systems considering emission problem. In Proceedings of the 40th Annual Conference of the IEEE Industrial Electronics Society, Dallas, TX, USA, 29 October 2014.
3. Hakimi, S.M.; Moghaddas-Tafreshi, S.M. Optimal planning of a smart microgrid including demand response and intermittent renewable energy resources. *IEEE Trans. Smart Grid* **2014**, *5*, 2889–2900. [CrossRef]
4. Grillo, S.; Marinelli, M.; Massucco, S.; Silvestro, F. Optimal management strategy of a battery-based storage system to improve renewable energy integration in distribution networks. *IEEE Trans. Smart Grid* **2012**, *3*, 950–958. [CrossRef]
5. Olowu, T.O.; Sundararajan, A.; Moghaddamicisions, M.; Sarwat, A.I. Future challenges and mitigation methods for high photovoltaic penetration: A survey. *Energies* **2018**, *11*, 1782. [CrossRef]
6. Sundararajan, A.; Olowu, T.O.; Wei, L.; Rahman, S.; Sarwat, A.I. Case study on the effects of the partial solar eclipse on distributed PV systems and management areas. *IEEE Trans. Smart Grid* **2019**, *2*, 477–490. [CrossRef]

7. Debnath, A.; Olowu, T.O.; Parvez, I.; Sarwat, A. A binary search algorithm based optimal sizing of photovoltaic and energy storage systems. In Proceedings of the IEEE Green Technologies Conference (GreenTech), Virtual Conference, 7–9 April 2021. [CrossRef]
8. Kaldellis, J.; Zafirakis, D.; Kondili, E. Optimum sizing of photovoltaic-energy storage systems for autonomous small islands. *Int. J. Electr. Power Energy Syst.* **2010**, *32*, 24–36. [CrossRef]
9. Li, J. Optimal sizing of grid-connected photovoltaic battery systems for residential houses in Australia. *Renew. Energy* **2019**, *136*, 1245–1254. [CrossRef]
10. Mohammed, A.Q.; Al-Anbarri, K.A.; Hannun, R.M. Optimal combination and sizing of a stand-alone hybrid energy system using a nomadic people optimizer. *IEEE Access* **2020**, *8*, 200518–200540. [CrossRef]
11. Tutkun, N.; Çelebi, N.; Bozok, N. Optimum unit sizing of wind-PV-battery system components in a typical residential home. In Proceedings of the 2016 International Renewable and Sustainable Energy Conference (IRSEC), Marrakesh, Morocco, 14–17 November 2016.
12. Nara, K.; Shiose, A.; Kitagawa, M.; Ishihara, T. Implement of genetic algorithm for distribution systems loss minimum re-configuration. *IEEE Trans. Power Syst.* **1992**, *7*, 1044–1051. [CrossRef]
13. Park, J.B.; Park, Y.M.; Won, J.R.; Lee, K.Y. An improved genetic algorithm for generation expansion planning. *IEEE Trans. Power Syst.* **2000**, *15*, 916–922. [CrossRef]
14. Fukuyama, Y.; Chiang, H.D. A parallel genetic algorithm for generation expansion planning. *IEEE Trans. Power Syst.* **1996**, *11*, 955–961. [CrossRef]
15. Ciornei, I.; Kyriakides, E. A GA-API solution for the economic dispatch of generation in power system operation. *IEEE Trans. Power Syst.* **2012**, *27*, 233–242. [CrossRef]
16. Park, Y.M.; Park, J.B.; Won, J.R. A hybrid genetic algorithm/dynamic programming approach to optimal long-term generation expansion planning. *J. Electr. Power Energy Syst.* **1998**, *20*, 295–303. [CrossRef]
17. Chun, J.S.; Jung, H.K.; Hahn, S.Y. A study on comparison of optimization performances between immune algorithm and other heuristic algorithms. *IEEE Trans. Magn.* **1998**, *34*, 2972–2975. [CrossRef]
18. Huang, S. An immune-based optimization method to capacaitor placement in a radial distribution system. *IEEE Trans. Power Deliv.* **2000**, *15*, 744–749. [CrossRef]
19. Toma, N.; Endo, S.; Yamanda, K. Immune algorithm with immune network and MHC for adaptive problem solving. In Proceedings of the IEEE International Conference on Systems, Man, and Cybernetic, Tokyo, Japan, 12–15 October 1999.
20. Kennedy, J.; Eberhart, R. Particle swarm optimization. In Proceedings of the IEEE International Conference on Neural Networks (ICNN'95), Perth, Australia, 27 November–1 December 1995.
21. Eberhart, R.; Shi, Y. Comparing inertia weights and constriction factors in particle swarm optimization. In Proceedings of the Congress on Evolutionary Computation (CEC2000), La Jolla, CA, USA, 16–19 July 2000.
22. Abido, M.A. Particle swarm optimization for multi-machine power system stabilizer design. In Proceedings of the IEEE Power Engineering Society Summer Meeting, Vancouver, BC, Canada, 15–19 July 2001.
23. Meraihi, Y.; Gabis, A.B.; Mirjalili, S.; Ramdane-Cherif, A. Grasshopper optimization algorithm: Theory, variants, and applications. *IEEE Access* **2021**, *9*, 50001–50024. [CrossRef]
24. Yang, X. Firefly algorithms for multimodal optimization. In Proceedings of the 5th International Symposium on Stochastic Algorithms (SAGA 2009), Sapporo, Japan, 26–28 October 2009.
25. Niknam, T.; Golestaneh, F. Enhanced bee swarm optimization algorithm for dynamic economic dispatch. *IEEE Syst. J.* **2013**, *7*, 754–762. [CrossRef]
26. Yang, X. A new metaheuristic bat-inspired algorithm. In *Nature Inspired Cooperative Strategies for Optimization (NICSO 2010)*; González, J.R., Pelta, D.A., Cruz, C., Terrazas, G., Krasnogor, N., Eds.; Springer: Berlin/Heidelberg, Germany, 2010; Volume 284, pp. 65–74.
27. Chen, S.L.; Zhan, T.S.; Tsay, M.T. Generation expansion planning of the utility with refined immune algorithm. *Electr. Power Syst. Res.* **2006**, *76*, 251–258. [CrossRef]
28. Lin, W.M.; Cheng, F.S.; Tsay, M.S. Distribution feeder reconfiguration with refined genetic algorithm. *IEE Proc.-Gener. Transm. Distrib.* **2000**, *147*, 349–354. [CrossRef]
29. Zhan, T.S.; Tsay, M.T. An improved genetic algorithm for the generation in electricity markets expansion planning of the utility in a competitive market. *Int. J. Eng. Intell. Syst.* **2004**, *12*, 167–173.
30. Lin, W.M.; Zhan, T.S. Multiple-frequency three-phase load flow for harmonic analysis. *IEEE Trans. Power Syst.* **2004**, *19*, 897–904. [CrossRef]
31. Lin, W.M.; Teng, J.H. Three-phase distribution network fast-decoupled power flow solution. *Int. J. Electr. Power Energy Syst.* **2000**, *22*, 375–380. [CrossRef]
32. Hou, J.C. Optimal Injection-Point Decision of the Photovoltaic Generation with Energy Storage System. Master's Thesis, Kao Yuan University, Kaohsiung City, China, 2019.